

Decoding the Roles of Amyloid- β (1–42)'s Key Oligomerization Domains toward Designing Epitope-Specific Aggregation Inhibitors

Dongjoon Im, Soohyeong Kim, Gyusub Yoon, Da Gyeong Hyun, Yu-Gon Eom, Ye Eun Lee, Chang Ho Sohn, Jeong-Mo Choi,* and Hugh I. Kim*



Cite This: *JACS Au* 2023, 3, 1065–1075



Read Online

ACCESS |



Metrics & More



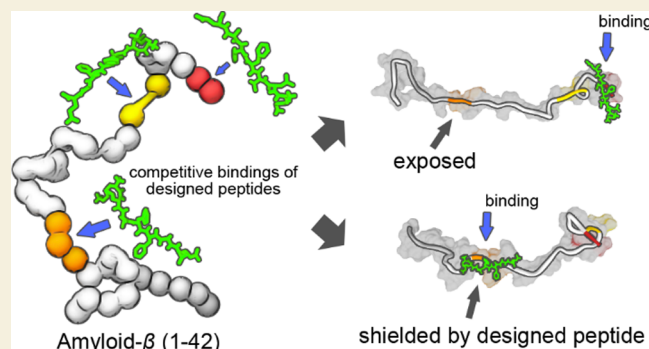
Article Recommendations



Supporting Information

ABSTRACT: Fibrillar amyloid aggregates are the pathological hallmarks of multiple neurodegenerative diseases. The amyloid- β (1–42) protein, in particular, is a major component of senile plaques in the brains of patients with Alzheimer's disease and a primary target for disease treatment. Determining the essential domains of amyloid- β (1–42) that facilitate its oligomerization is critical for the development of aggregation inhibitors as potential therapeutic agents. In this study, we identified three key hydrophobic sites ($^{17}\text{LVF}^{19}$, $^{32}\text{IGL}^{34}$, and $^{41}\text{IA}^{42}$) on amyloid- β (1–42) and investigated their involvement in the self-assembly process of the protein. Based on these findings, we designed candidate inhibitor peptides of amyloid- β (1–42) aggregation. Using the designed peptides, we characterized the roles of the three hydrophobic regions during amyloid- β (1–42) fibrillar aggregation and monitored the consequent effects on its aggregation property and structural conversion. Furthermore, we used an amyloid- β (1–42) double point mutant (I41N/A42N) to examine the interactions between the two C-terminal end residues with the two hydrophobic regions and their roles in amyloid self-assembly. Our results indicate that interchain interactions in the central hydrophobic region ($^{17}\text{LVF}^{19}$) of amyloid- β (1–42) are important for fibrillar aggregation, and its interaction with other domains is associated with the accessibility of the central hydrophobic region for initiating the oligomerization process. Our study provides mechanistic insights into the self-assembly of amyloid- β (1–42) and highlights key structural domains that facilitate this process. Our results can be further applied toward improving the rational design of candidate amyloid- β (1–42) aggregation inhibitors.

KEYWORDS: peptides and proteins, conformation, oligomers, aggregation, inhibitors



INTRODUCTION

Pathogenic amyloid aggregation of intrinsically disordered proteins (IDPs) is related to multiple neurodegenerative diseases.¹ The pathological hallmark of Alzheimer's disease (AD)—which is the most prevalent type of dementia—is the accumulation of amyloid- β ($A\beta$) and microtubule-associated protein (MAP) tau.^{2,3} Fibrillar aggregation of $A\beta$ leads to the formation of senile plaques in the brains of AD patients.⁴ Numerous reports, including genome-wide association studies, imply that the appearance of amyloid aggregates is closely related to neurodegeneration.⁵ Nevertheless, the exact pathophysiological role of the $A\beta$ protein remains unclear.

The $A\beta$ proteins are formed by enzymatic cleavage of the amyloid precursor protein (APP) and commonly have 40 or 42 residues ($A\beta_{40}$ and $A\beta_{42}$, respectively).⁶ The longer $A\beta_{42}$ tends to favor hydrophobic interaction-mediated self-assembly more so in comparison with $A\beta_{40}$.⁷ The $A\beta$ proteins form various oligomeric species, and each species facilitates the subsequent assembly of several intermediates, eventually culminating in the formation of mature fibrils.⁸ Although

multiple studies have presented evidence that the $A\beta$ protein promotes neuronal cell death and hyperphosphorylation of MAP tau, the molecular mechanism of amyloid aggregation is yet to be clearly elucidated owing to the highly heterogeneous nature of the pathological cascade.^{9,10} To date, antibodies and small molecules that selectively bind to aggregates of $A\beta$ fibrils have been introduced as potential therapeutic agents for AD.¹¹ In addition, a number of drug candidates target the $A\beta$ -related pathway, which regulates the production or existence of $A\beta$ and modulates the ratio of $A\beta$ proteins.¹² Although many potential drug candidates against pathogenic amyloid aggregates have been proposed for AD treatment, their effectiveness remains debatable. Therefore, it is necessary to develop a more

Received: December 7, 2022

Revised: February 22, 2023

Accepted: February 22, 2023

Published: March 2, 2023



potent therapeutic strategy for AD based on a more in-depth understanding of the fibrillar amyloid aggregation process at a molecular level.

Recent studies have attempted to rationally design candidate drugs in order to improve existing therapeutic approaches or suppress the fibrillar amyloid aggregation process altogether^{13–16} based on the accumulated knowledge of interlinked dynamics of IDPs, intermediate oligomers, and their pathogenesis to date.^{17–20} For example, a pharmacophore in MAP tau for the binding of small molecules was shown to enhance the binding of potential therapeutic agents.¹⁵ In addition, an epitope-specific method for antibody design has been reported, which allows development of antibodies to the desired binding epitopes of amyloidogenic IDPs.¹⁶ Since the self-assembly property of A β can be modulated by interrupting or enhancing the contact of the hydrophobic core domains, it would be possible to target the hydrophobic core regions in order to prevent or reduce the capacity of A β for self-assembling. Based on such findings, as well as in silico and in vitro analyses, we have previously shown that rationally designed point mutants of A β 42 can suppress fibrillar aggregation.¹⁴ In particular, we identified two hydrophobic residues (Phe19 and Ile32) which are crucial for facilitating oligomerization of A β 42.¹⁴ The designed point mutants against those sites cross-interacted with A β 42 in early-stage amyloid aggregation and interfered with the A β 42 self-assembly.¹⁴

In this study, we aimed to identify the target region responsible for disrupting fibrillar amyloid aggregation of A β 42 and further delineate its role in this process. We employed a machine learning (ML) algorithm to predict the binding domain of prefibrillar A β 42 with various fragments of A β 42.²¹ Next, we selected two A β 42 fragments [¹⁶KLVEFAE²², referred to as fragment a (F_a), and ²⁵GSNKGAIIGLM³⁵, referred to as fragment b (F_b), respectively], which displayed self-assembly properties, while also containing one of the two crucial hydrophobic residues (Phe19 and Ile32). Moreover, we designed candidate inhibitor peptides against fibrillar amyloid aggregation of A β 42 using the two selected fragments and applied a point mutation strategy to eliminate their self-assembly properties. We also confirmed the suppressive effects of the inhibitor candidates on amyloid cluster formation and the alleviation of A β 42-dependent cytotoxicity in vitro using an SH-SY-5Y cell line. In addition, we examined the disassembly of preformed A β 42 fibrils upon co-incubation with the inhibitor candidates. To understand the molecular mechanisms underlying the suppression of A β 42 aggregation, we investigated the interference of inhibitor candidates in early-stage aggregation using an interdisciplinary biophysical approach. Hydrogen–deuterium exchange mass spectrometry (HDX-MS) and ion mobility mass spectrometry (IM-MS) provided evidence of the structural conversion of A β 42 by designed inhibitor candidates. Combining ML algorithm predictions of peptide-inhibitor complex structures with comprehensive molecular dynamics (MD) simulations provided the molecular basis for peptide-inhibitor interactions. The in silico results and the electron transfer dissociation mass spectrometry (ETD-MS) analysis revealed the binding sites of the inhibitor candidates on A β 42. We also performed small-angle X-ray scattering (SAXS)-based modeling of the A β 42 ensembles to understand the solution-phase structural dynamics of A β 42. Finally, in order to delineate the role of the A β 42 C-terminal end in amyloid aggregation, we utilized a mutant isoform of

A β 42, I41N/A42N, in which the two C-terminal hydrophobic residues were substituted with polar amino acids.

EXPERIMENTAL SECTION

Predictions of Complex Structures

To predict the complex structures of A β 42 and its fragments or peptide inhibitor candidates, we employed the AlphaFold multimer (version 2.1.1).²¹ Source code is available at <https://github.com/deepmind/alphafold>. Structural images were created using UCSF Chimera (version 1.16).²²

ThT Fluorescence Assay

Thioflavin T (ThT) assays were used to track the amyloid aggregation of A β 42 proteins in the presence or absence of the designed peptides. The concentration of A β 42 was set at 2 and 5 μ M. ThT was incubated at 37 °C without agitation in 20 mM Tris–HCl buffer (pH 7.4) in SPL 96-well black microplates (SPL Life Science, Seoul, Korea) with sealing (EASYseal sealing film, Greiner-Bio-One). The designed peptide inhibitor candidates were applied in 1:1, 1:5, or 1:25 molar ratios. Fluorescence intensity was measured continuously at 1 h intervals, for up to 48 h using a Synergy H1 microplate reader (BioTek, Winooski, VT, USA) with excitation and emission wavelengths of 446 and 482 nm, respectively, from the top of the plate. The ThT assays for the I41N/A42N mutant were performed under the same experimental conditions, except for the A β 42 I41N/A42N concentration (10 μ M).

Transmission Electron Microscopy

Transmission electron microscopy (TEM) images of the A β 42 fibrils were obtained using negative staining protocols (Supporting Information). Briefly, incubated fibril samples (5 μ L) were spotted on a Cu(II) grid for 3 min at 20 °C and removed. The grids were washed twice with HPLC-grade water immediately after sample removal. Then, each sample was stained with 5 μ L of uranyl acetate solution (0.5% w/v) for 1 min. The samples were dried for 4 h at 20 °C after removal of the uranyl acetate solution. The TEM images were recorded using a JEM-F200 (TFEG; JEOL Ltd., Japan) field-emission transmission electron microscope [National Center for Inter-University Research Facilities (NCIRF), Seoul National University, Seoul, Republic of Korea] at various magnifications (200 kV; 6000 \times , 15,000 \times , 30,000 \times , and 60,000 \times magnification).

Cell Viability Test

MTT assay was used to determine cell viability. In each well of a 96-well plate, SH-SY-5Y cells (15,000 cells) were seeded and incubated for 24 h. Cells were treated with preincubated fibrils in DMEM for 48 h. The MTT solution (5 mg/mL) was added to the medium and incubated for 3 h at 37 °C to form blue MTT-formazan products which were assessed by measuring absorbance at 540 nm using a microplate reader. To ensure reproducibility, each set was tested in triplicate, and the assay was repeated three times.

Disassembly of Preformed Fibrils

A β 42 (10 μ M) was incubated for 24 h at 37 °C without agitation in 20 mM Tris–HCl buffer (pH 7.4). Fibrillar amyloid aggregation of A β 42 proteins (10 μ M) was monitored using a ThT fluorescence assay. The peptide inhibitor candidates were applied to the preformed fibrils of A β 42 (diluted to a concentration of 2 μ M), and the final peptide inhibitor candidate concentration was 50 μ M. Except for the addition of the peptide inhibitor candidate, the control fibrils from the same preformed fibrils of A β 42 were treated identically. All the samples were incubated at 37 °C without agitation for 24 h. Disassembly of preformed fibrils was monitored by endpoint ThT fluorescence intensity and TEM image analysis at various magnifications (6000 \times , 15,000 \times , 30,000 \times , and 60,000 \times magnification). The density of the fibrillar aggregates was calculated using the area fraction covered by fibrils in the TEM images. TEM images were further analyzed using the ImageJ software to determine fibril density. Six images at 6000 \times magnification were processed using MATLAB (version R2020a). The adaptthresh and wiener2 functions were used

to implement the adaptive thresholding and noise reduction steps, respectively.

Small-Angle X-ray Scattering

Solution SAXS experiments were carried out at the 4C SAXS II beamline at the Pohang Accelerator Laboratory (Pohang, Republic of Korea).²³ All SAXS experiments used freshly prepared samples. Ensemble structures were modeled using EOM analysis from the ATSAS software package (version 3.0.3).²⁴ External pools were generated by REMD simulations and used when running a genetic algorithm to optimize ensembles (GAJOE). The ensemble size was set at 50 curves per ensemble, and repetitions were not permitted. The experimental details are described in the [Supporting Information](#).

MD Simulations

MD simulations and umbrella sampling were performed using the GROMACS software package (version 2020.4).²⁵ To estimate the interchain contact probability between the A β 42 and each peptide inhibitor candidate, a REMD simulation (33 replicas, 150 ns) was performed for each complex system using the CHARMM36m force field and the TIP3P solvent model.^{26,27} The binding free energy was calculated using umbrella sampling combined with a pulling simulation. This was performed using the same force field and solvent model as described above. The 600 ps pulling simulation trajectories were divided into 30 windows, and the MD simulation was run for 10 ns in each window. External generation for EOM analysis was performed using the GROMACS software package (version 4.5.5) with the CHARMM36m force field and the General Born implicit solvation model, where five replicas were simulated for 20 ns.^{25,26,28} The DSSP program was used to calculate the solvent-accessible surface area (SASA) per residue as well as the total hydrophobic or hydrophilic surface area (gmx do_dssp module).

ESI-MS Combined with the HDX Technique

Freshly prepared A β 42 and peptide inhibitor candidates were deuterated with D₂O before quenching with formic acid. The final concentrations of A β 42 and the peptide inhibitor candidates were 10 and 50 μ M, respectively. The samples were immediately injected into a Synapt G2-Si HDMS quadrupole time-of-flight (Q-TOF) mass spectrometer (Waters, Manchester, UK) after the quenching agent was added. The backward-exchanged hydrogens were corrected with D₂O-hydrated fully deuterated A β 42.

Ion Mobility Mass Spectrometry

IM-MS was performed in the positive ion mode on a Synapt G2-Si HDMS Q-TOF mass spectrometer (Waters, UK, Manchester). The final concentration of the A β 42 protein was 10 μ M in 20 mM ammonium acetate (pH 6.8). The designed inhibitors were applied at a concentration of 50 μ M, and the proteins were transferred to the gas phase using an electrospray ionization (ESI) source. The ESI parameters and detailed descriptions for calibrating the collision cross-section are given in the [Supporting Information](#).

Electron Transfer Dissociation Mass Spectrometry

ETD was performed using a Synapt G2-Si HDMS Q-TOF mass spectrometer with ETD functionality (Waters, UK; Manchester). A β 42 and each peptide inhibitor candidate were mixed at concentrations of 10 and 50 μ M, respectively. The samples were introduced at a flow rate of 10 μ L/min using an ESI source. To generate anions, the ETD reagent 1,4-dicyanobenzene was introduced into the glow-discharge source. Anions were refilled in the trap cell for 0.2 s at a time interval of 1 s. The ETD mode parameters were a 0.2 V trap wave height, 14 mL/min trap gas flow, and 475 V ETD RF trap. Peak assignment was performed manually by comparing it to a fragment list generated by the ProteinProspector web server (<https://prospector.ucsf.edu/prospector/mshome.htm>). To compare the MD simulation and ETD-MS results, an interchain contact probability map of the complexes was projected onto the *x*-axis and overlaid on the ETD-MS results.

RESULTS

Design of Amyloid Aggregation Inhibitors

Recent crystallography studies have revealed that the hydrophobic domains of A β 42 form a hydrophobic core in the fibrillar structure of A β 42.²⁹ Prompted by previous findings, we designed novel point mutants of A β 42 to suppress its self-assembly property.¹⁴ Among the four selected residues (Phe19, Ile32, Leu34, and Ala42), our results showed that Phe19 and Ile32 were essential for fibrillar amyloid aggregation as amino acid substitutions in these positions effectively disrupted the process.¹⁴ Therefore, we hypothesized that the region including one of the two crucial residues plays a key role in suppressing fibrillar amyloid aggregation of A β 42. The previously reported mutant D1 (F19N/I32N) cross-interacts with wild-type A β 42 during early-stage oligomerization and as such interferes with fibrillar amyloid aggregation of A β 42 ([Figure 1a](#)).¹⁴ Herein, we aimed to identify the key domain which can effectively inhibit A β 42 aggregation and to target that region by using smaller A β 42 fragments to modulate the self-assembly function of A β 42.

Our criteria were that smaller A β 42 fragments must have self-assembly properties and include at least one of the essential residues (Phe19 or Ile32). To systematically search for binding domains, we compiled previously reported small fragments of A β 42 (F_a to F_q, 17 fragments in total) and employed AlphaFold to predict the binding of each fragment to prefibrillar A β 42 ([Figures 1b](#) and [S1](#) and [Table S1](#)).^{30–39} The A β 42 tetramer is predicted to stack in parallel, and the fragment peptide KLVFFAE (F_a) is expected to bind to its cognate region (¹⁶KLVFFAE²²) in a parallel conformation. The peptide fragment GSNKGAIIGLM (F_b) also associates with the central hydrophobic region of A β 42. However, most of the N-terminal fragments of A β 42 were expected to bind to the C-terminal end of A β 42 ([Figure S1](#), F_h–F_q). A short fragment, such as IIGLM, also bound to the C-terminal end of A β 42 ([Figure S1](#), F_g). Several of the fragments we examined reportedly demonstrated self-assembly properties, and as such, they were expected to bind to the central hydrophobic region.^{30,31} Therefore, we posited that targeting the central hydrophobic region using fragment-based inhibitor candidates could be effective in disrupting the amyloid aggregation process.

Based on the predictions from AlphaFold, we selected two short, aggregate-prone peptides, F_a and F_b, along with their point mutants, to target each domain of A β 42 with their corresponding sequences while monitoring their effectiveness in inhibiting A β 42 amyloid aggregation ([Figure 1a](#)). The peptides F_a and F_b both include the mutation target sites mentioned above and are also specific for the central and C-terminal regions, respectively. These two peptides have been reported to form insoluble amyloid bodies in vitro and are widely used as model systems in amyloid aggregation studies.^{30,31} We monitored the cluster formation of the two fragments using a ThT fluorescence assay, whose fluorescence intensity increases upon binding to amyloid fibrils, and found that both fragments have self-assembly capabilities ([Figure S2](#)). As the intermolecular contacts are mainly initiated by hydrophobic interactions, we expected that each fragment with self-assembly properties would still be able to cross-interact with A β 42 via the corresponding domain.

We chose KLVNFAEDVGSNKGAIIGLM (P_{ab}) as our first experimental inhibitor candidate peptide because it spans both

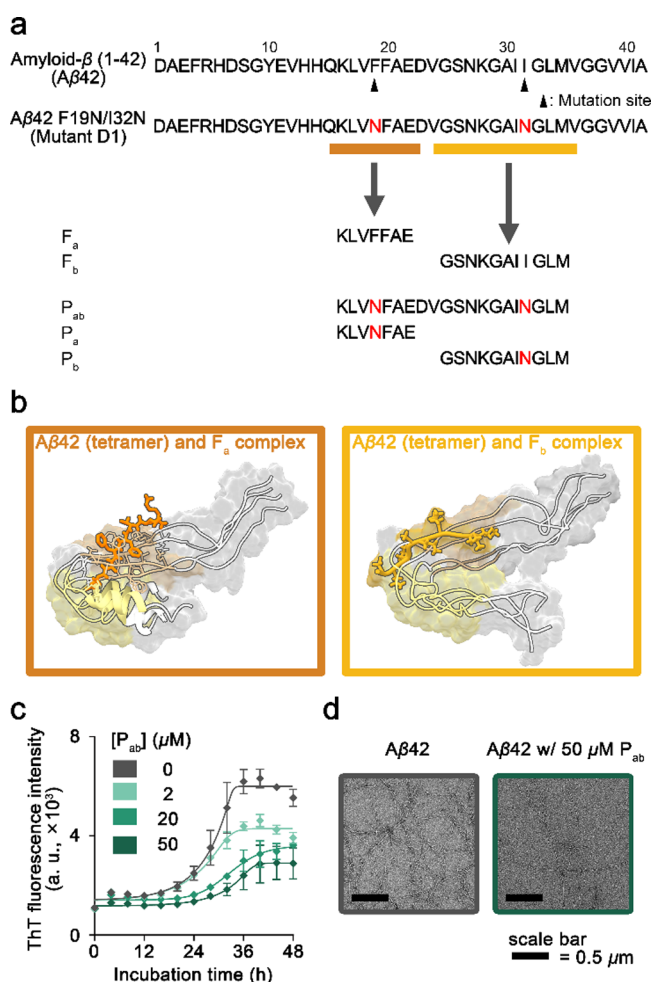


Figure 1. Design of amyloid aggregation inhibitors for amyloid- β (1–42) (A β 42). (a) Domains of interest are indicated by underlining, and the amino acid sequences of A β 42 fragments (F_a and F_b) and peptide inhibitor candidates (P_{ab}, P_a, and P_b) are shown. (b) AlphaFold-predicted structures of the peptide fragment complexes. The A β 42 tetramer is predicted to stack in parallel, and the fragments (F_a and F_b) are expected to bind to the central hydrophobic region. The central hydrophobic region of A β 42 (¹⁶KLVFFAE²²) is colored as tan, ²⁵GSNKGAIIGLM³⁵ of A β 42 as khaki, and each fragment, F_a and F_b, as orange and yellow, respectively. (c) ThT incubation assay for the aggregation kinetics of A β 42 and mixtures of A β 42 and peptide inhibitor candidate P_{ab}. (d) TEM images of A β 42 fibrils in A β 42 and mixtures of A β 42 and P_{ab}. The error bars represent the standard deviation from three independent experiments.

the ¹⁶KLVFFAE²² (F_a) and ²⁵GSNKGAIIGLM³⁵ (F_b) regions and contains both F19N and I32N point mutations (Figure 1a). The suppressive effect of the designed peptide inhibitor candidate P_{ab} on A β 42 amyloid aggregation was monitored by a ThT incubation assay and TEM image analysis after negative staining (Figure 1c,d). The A β 42 sample showed an increase in the ThT fluorescence intensity as a function of time. The mixture of A β 42 and P_{ab} at equimolar concentrations displayed lower ThT fluorescence intensity than the A β 42 sample at plateau intensity. In addition, the peptide inhibitor candidate P_{ab} suppressed fibrillar amyloid aggregation in a concentration-dependent manner (Figure 1c). The TEM image analysis supports our ThT assay results, showing fewer amyloid fibrils in the mixture of A β 42 and P_{ab} (Figure 1d).

Effects of Fragments and Designed Peptides on Fibrillar Amyloid Aggregation of A β 42

To understand the specific effects of different regions on fibrillar amyloid aggregation, we further examined how the aggregation of A β 42 is affected by two smaller peptide inhibitor candidates, KLVNFAE (P_a) and GSNKGAIIGLM (P_b), which span the central and C-terminal hydrophobic regions, respectively. While both P_a and P_{ab} suppressed A β 42 aggregation to an extent, P_{ab} was more effective in this regard than P_a (Figures 1c and 2a,c). Interestingly, the inhibitor candidate P_b did not suppress A β 42 aggregation (Figure 2b,c). The TEM image analysis agreed with the ThT assay results, suggesting an inhibitory effect of P_a on A β 42 aggregation, while no considerable effect was observed for P_b. Notably, both P_{ab} and P_a, which contain the F19N point mutation, effectively suppressed A β 42 amyloid aggregation (Figures 1d and 2d). We further investigated the inhibitory effect of designed peptides on A β 42 aggregation at higher A β 42 concentration (25 μ M) since distinct forms of the A β oligomer have been reported above the critical concentration (20–25 μ M).^{40,41} The results show that even though the A β 42 concentration increased, the suppressive effect of the designed peptides persisted (Figure S6).

To monitor the cellular responses after addition of the designed inhibitor candidates, we performed the cytotoxicity test on the SH-SY-5Y cells using the modified thiazolyl blue tetrazolium bromide (MTT) (Figure 2e). We incubated the pure A β 42 sample, as well as mixtures of A β 42 and the designed peptides for 48 h at 37 °C, and applied these to SH-SY-5Y cells. The results showed that the cytotoxicity of A β 42 decreased significantly as the concentration of P_{ab} increased. The inhibitor candidate P_a also alleviated the cytotoxicity of A β 42 in a concentration-dependent manner. In contrast, P_b did not significantly diminish the cytotoxicity of A β 42. These findings indicated that suppression of A β 42 aggregation by the designed peptide inhibitors, P_{ab} and P_a, also reduced the toxicity of A β 42 (Figures 1c and 2a,e).

Moreover, we assessed the disassembly of amyloid A β 42 clusters using these three peptides. After a 24 h incubation period, we applied the designed peptides to the preformed A β 42 fibrils and allowed these to act for a further 24 h at 37 °C. The TEM image analysis revealed that the designed peptides affected the density of the fibrillar aggregates (Figure 2f,g). The area fraction covered with fibrils in the TEM images was used to calculate the density of fibrillar aggregates. The density of fibrillar aggregates in the TEM images of the A β 42 sample was 3.45%, and this decreased to 1.48, 2.82, and 3.01% upon addition of P_{ab}, P_a, and P_b, respectively (Figure 2f). The endpoint ThT fluorescence intensity of each sample was monitored to quantify ThT-positive aggregates. Compared to the A β 42 sample treated with incubation buffer (as a negative control), the ThT fluorescence intensity in each of the A β 42-inhibitor mixture samples treated with either P_{ab}, P_a, and P_b decreased to 68, 81, and 92%, respectively (Figure 2h). The designed peptide P_{ab}, which covered both the F_a and F_b regions in A β 42 and included F19N and I32N point mutations, induced the disassembly of preformed amyloid aggregates of A β 42. The P_a designed peptide, which covers the F_a region in A β 42 and includes an F19N point mutation, seemed to have similar trends to P_{ab}. However, P_b, the sequence of which corresponds to that of F_b and contains an I32N point mutation, did not show notable disassembly of the preformed amyloid aggregates of A β 42. The MTT assay showed alleviated

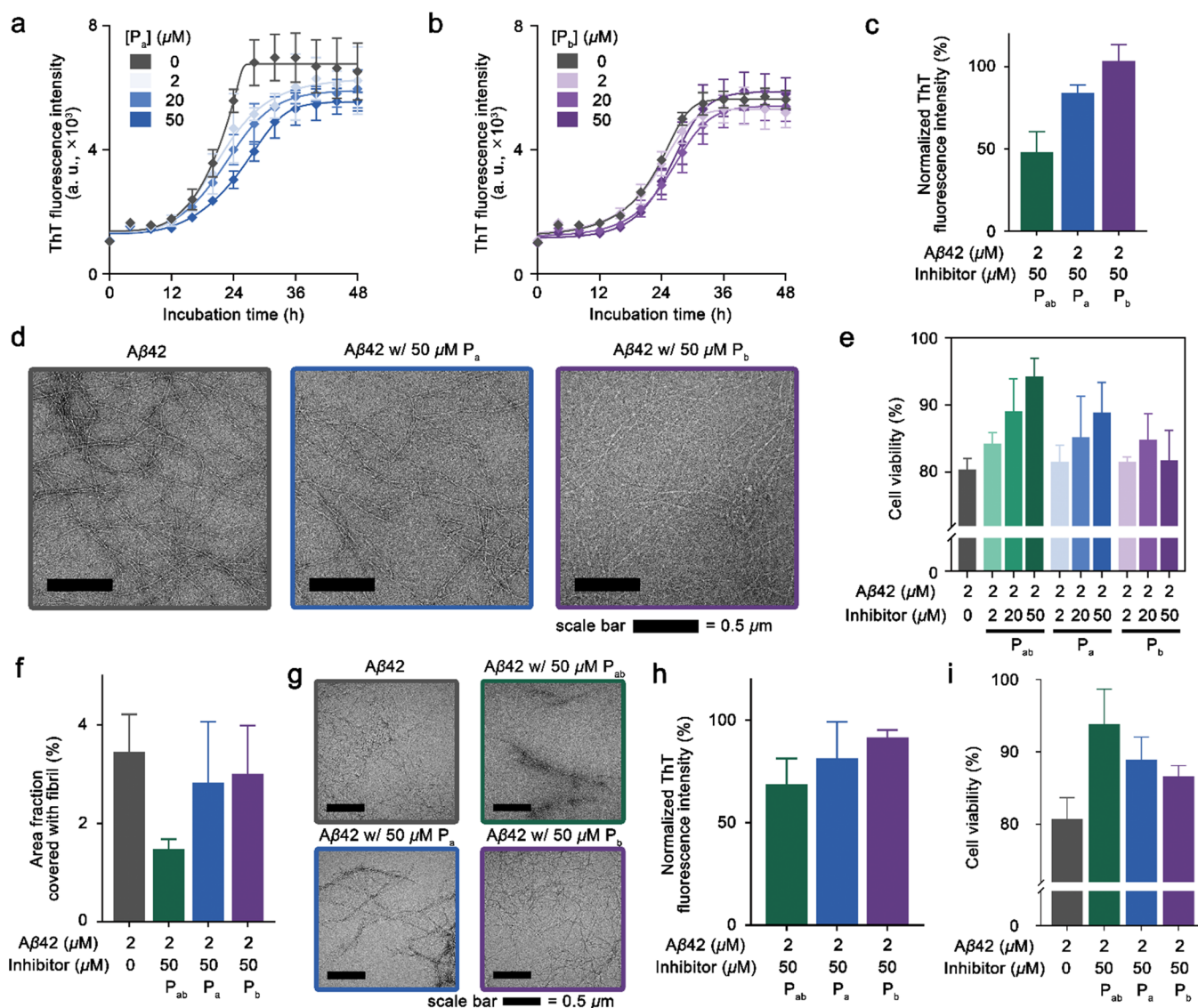


Figure 2. Effects of peptides and inhibitor candidates on fibrillar amyloid aggregation of A β 42. ThT fluorescence assays were used to monitor the aggregation kinetics of the mixture of A β 42 and (a) P_a or (b) P_b . (c) Normalized ThT fluorescence intensity of A β 42 and the mixture of A β 42 with inhibitor candidates after 48 h incubation. (d) TEM images of A β 42 fibrils in mixtures of A β 42 and peptide inhibitor candidates. (e) MTT assay to monitor the cytotoxicity of A β 42 and mixtures of A β 42 with the three designed mutant candidates. The samples were preincubated for 48 h and added to the SH-SY5Y cells, followed by an additional 48 h incubation. (f, g) Disassembly of preformed A β 42 fibrils monitored by TEM image analysis. Designed inhibitor candidates added to preformed fibrils and incubated 24 h at 37 $^{\circ}$ C. (h) Normalized ThT fluorescence intensity at the endpoint of the disassembly assay. (i) MTT assay to monitor the cytotoxicity of preformed A β 42 fibrils after inhibitor-induced disassembly. The error bars represent the standard deviation from three independent experiments, except for fibril density analysis (standard deviation from six images).

cytotoxicity of preformed A β 42 fibrils after inhibitor-induced disassembly, and the results were in good agreement with our fibril disassembly assays (Figure 2i).

Identification of the Three Key Domains of A β 42

To understand the different roles of the three regions (central hydrophobic region, 17 LVF 19 , Φ_1 ; C-terminal hydrophobic region, 32 IGL 34 , Φ_2 ; and C-terminal end, 41 IA 42 , Φ_3) (Figure S7), we investigated the solution-phase dynamics of A β 42 using SAXS experiments. We performed an ensemble optimization method (EOM) analysis since the Kratky plot showed that A β 42 has a highly unstructured conformation (Figure 3a), and the theoretical analysis was well fitted to the experimental curve ($R_{g,theo} = 22.40 \pm 3.19$ Å and $R_{g,exp} = 22.81 \pm 1.25$ Å, respectively) (Figure 3b). Fifty ensemble structures

of A β 42 were obtained from EOM analysis (Figure 3c) and subjected to calculations for the intramolecular contacts of each structure. The resulting intramolecular distances were plotted as a contact probability map of A β 42 to better understand the transient interactions in the monomeric state of A β 42 (Figure 3d). We observed that the Φ_2 A β 42 site interacts with both Φ_1 and Φ_3 on the same molecule. The interaction between Φ_2 and Φ_3 should be avoided for the successful association of Φ_1 with Φ_2 . The latter interaction shields the Φ_1 domain by positioning it inward in the A β 42 structure. Based on these observations, we speculate that the structural fluctuations of A β 42 originate from intramolecular hydrophobic interactions in the C-terminal regions.

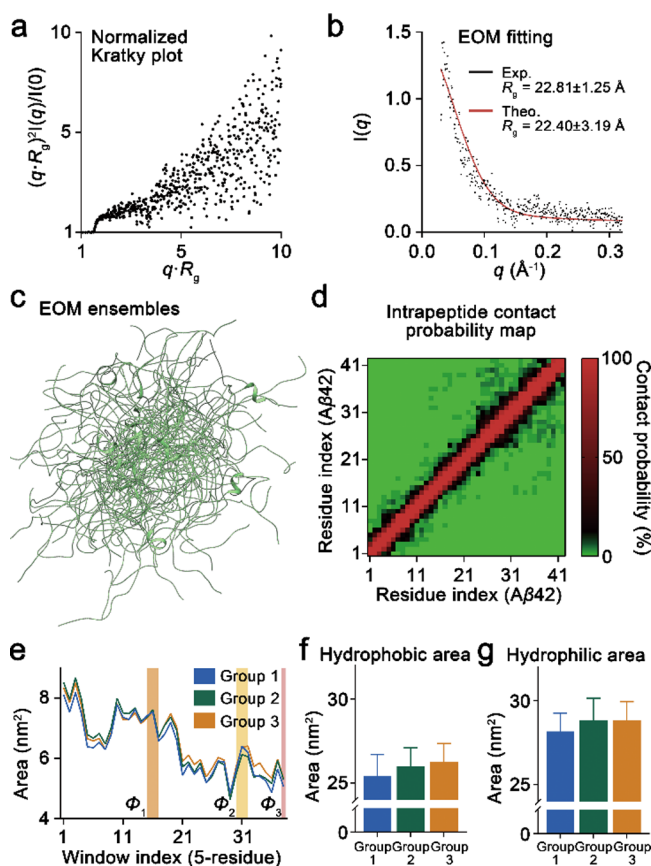


Figure 3. Modeling of solution-phase amyloid- β (1–42) ($A\beta_{42}$) ensembles using SAXS. (a) Normalized Kratky plot of $A\beta_{42}$ based on the SAXS profile. (b) EOM analysis of the raw SAXS profile of $A\beta_{42}$ (black) and the fitted curve (red). (c) Ensemble structures of $A\beta_{42}$ obtained using EOM analysis. (d) EOM-derived intrapeptide contact probability map of the $A\beta_{42}$ ensembles. (e) 50 EOM structures are divided into three groups by the radius of gyration, and the SASA of the adjacent five residues is plotted. Window 1 means residues 1–5, and window 2 means residues 2–6. (f, g) Averaged SASA calculated from three groups of EOM structures with (f) hydrophobic and (g) hydrophilic areas. The error bars represent the standard deviation.

We separated the modeled ensembles into three groups according to the radius of gyration (compact conformers were assigned to group 1, intermediates to group 2, and extended conformers to group 3) to deconvolute the structural basis of the $A\beta_{42}$ fluctuations (Figure S8). We assessed the exposure of each domain (5-residue windows) based on SASA (Figure 3e). These results suggest that Φ_2 is mostly located in the interior sites of the protein; thus, Φ_1 is likely exposed to solvent molecules and other $A\beta_{42}$ peptides. The total solvent-accessible hydrophobic surface area decreased in proportion to the radius of the $A\beta_{42}$ gyration (Figure 3f). The sum of the solvent-accessible hydrophilic surface area also decreased in group 1, which suggests that compact conformations of $A\beta_{42}$ lead to the shielding of both hydrophobic and hydrophilic surface areas (Figure 3f,g). On the other hand, the intermediate conformers of $A\beta_{42}$ did not induce shielding of the hydrophilic surface area, which indicates that the structural fluctuations of $A\beta_{42}$ conformers are mainly driven by intramolecular contacts of the hydrophobic regions (Figure 3g). Investigation of the solution-phase dynamics of $A\beta_{42}$ revealed the interactions between its three key domains (Φ_1 , Φ_2 , and Φ_3). These observations showcase that the deviation

in the solvent-accessible area between groups 2 and 3 mainly arises from two intramolecular hydrophobic interactions: between Φ_1 and Φ_2 or between Φ_2 and Φ_3 (Figure 3e–g). We previously reported that self-assembly of $A\beta_{42}$ initiates with the interchain hydrophobic contacts of Φ_1 and Φ_2 .¹⁴ Intramolecular hydrophobic interaction between Φ_1 and Φ_2 leads to shielding of both interchain interaction sites. However, when Φ_2 interacts with Φ_3 , the Φ_1 domain is consequently exposed. Based on these findings, we hypothesized that Φ_1 is shielded by Φ_2 , thereby delaying fibrillar amyloid aggregation. As such, it may be possible that the shielding effect of Φ_2 could be weakened when the domain interacts with Φ_3 .

Molecular Mechanisms Underlying Suppressed Amyloid Aggregation of $A\beta_{42}$

We performed MS-based structural analyses to further investigate the molecular mechanisms underlying the suppression of the fibrillar amyloid aggregation process. The deuteration level of proteins during HDX reflects the accessibility of protein regions to solvent molecules. A higher HDX propensity indicated more frequent solvent exposure with an extended conformation. We employed HDX-MS analysis to monitor the structural conversion of $A\beta_{42}$ in the presence of the designed peptides (Figure 4a). As a reference, the increment in the deuteration level of inhibitor-free $A\beta_{42}$ (incubated for 1 s in water prior to acidic quenching) during the MS data acquisition for 90 s was $1.07 \pm 0.21\%$. All three designed inhibitor candidates facilitate $A\beta_{42}$ deuteration, with P_b causing the greatest increase in $A\beta_{42}$ deuteration level (1.72 ± 0.01 , 1.63 ± 0.21 , and $1.94 \pm 0.38\%$ for P_{ab} , P_a , and P_b , respectively). Therefore, it is anticipated that the designed peptides, in general, induce $A\beta_{42}$ to be extended by peptide–protein interactions.

Next, we attempted to dissect the interaction modes of the $A\beta_{42}$ complexes with different peptides. The structural dynamics of $A\beta_{42}$ and $A\beta_{42}$ –inhibitor complexes were monitored in the gas phase using IM-MS by determining the collision cross-sections (CCSs) of each complex ion (Figure 4b). According to the IM spectra, the complex ions (+4 charge state) showed increased CCS values compared to free $A\beta_{42}$ ions. The complex ions of $A\beta_{42}$ with P_a or P_b showed two conformers (compact and extended conformers), while the $A\beta_{42}$ complex ion with P_{ab} did not show extended conformers (Figure 4b). It should be noted that the compact conformer of the $A\beta_{42}$ –inhibitor complex ion is still extended compared to the intact $A\beta_{42}$ ion's conformer (Figure 4a,b). The $A\beta_{42}$ – P_a complex ions preferred a compact conformation over the extended conformation. In contrast, the P_b -bound complex ions displayed an increase in the population of extended conformers. Taken together, the $A\beta_{42}$ – P_{ab} complex ions presented only with a compact conformer, while $A\beta_{42}$ complexes with the other designed peptides showed both compact and extended conformers. In addition, the $A\beta_{42}$ complex ions with P_a and P_b showed extended conformers to a significant extent. The $A\beta_{42}$ – P_b complex ions displayed a preferential tendency for extended conformers in contrast to the $A\beta_{42}$ – P_a complex. The degree of extension of $A\beta_{42}$ may play an important role in suppressing the fibrillar amyloid aggregation of $A\beta_{42}$.

To further investigate the atomistic details of the observed structural changes in $A\beta_{42}$ and various amyloid complexes, we utilized AlphaFold to predict complex structures between the $A\beta_{42}$ monomer and each of the three designed peptides. The

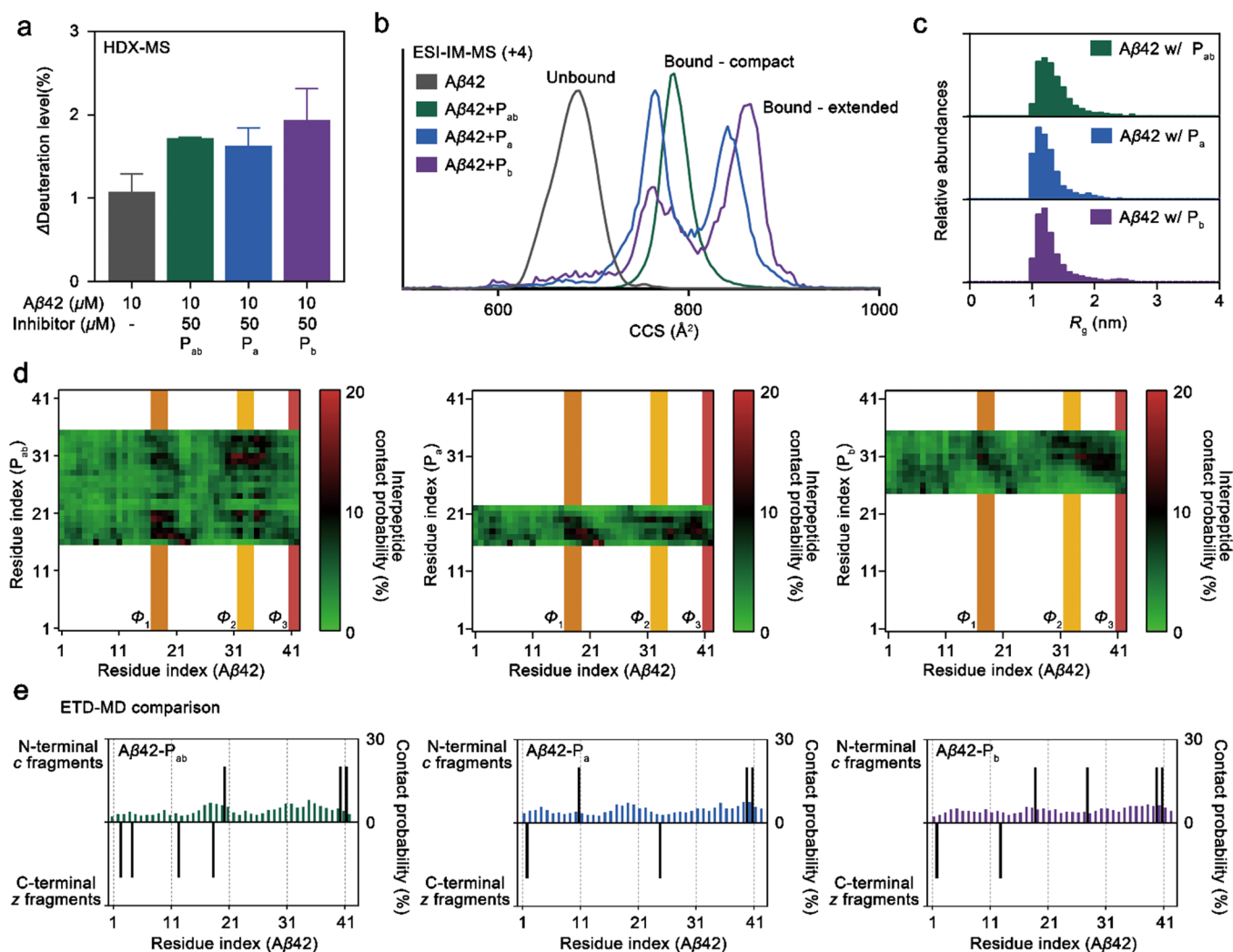


Figure 4. Investigation of the structural dynamics of the amyloid- β (1–42) ($A\beta_{42}$) after the addition of the three designed inhibitor candidates. (a) Increment in the normalized deuteration level for $A\beta_{42}$ with and without the addition of the designed inhibitor candidates. (b) Distributions of experimental collision cross-section (Ω_D) of $A\beta_{42}$ and $A\beta_{42}$ -inhibitor complexes. (c) R_g distributions of the $A\beta_{42}$ conformers obtained from the REMD simulations of $A\beta_{42}$ -inhibitor complexes. (d) Interpeptide contact probability maps of the three $A\beta_{42}$ -inhibitor complexes from 24.75 μ s MD simulations. (e) Comparison of the residue-specific interpeptide contact probabilities obtained from MD simulations and bindings between $A\beta_{42}$ and inhibitor candidates, which were monitored by using ETD-MS fragmentation of the $A\beta_{42}$ -inhibitor complex. The product ions are indicated in gray, and the MD simulated contact probability is represented in green, blue, and purple ($A\beta_{42}$ - P_{ab} , $A\beta_{42}$ - P_a , and $A\beta_{42}$ - P_b , respectively). The error bars represent the standard deviation from three independent experiments.

major binding site was the central hydrophobic region of $A\beta_{42}$ (Figure S11). The complex structures were fed into replica-exchange MD (REMD) simulations as initial structures. The REMD simulation sets consisted of 33 different temperatures ranging from 300 to 400 K with equal exchange probabilities. For each designed peptide, we obtained five R_g distributions of $A\beta_{42}$ and five interpeptide contact probability maps from independent REMD simulations and weight-averaged them based on the binding free energy obtained by umbrella sampling (Table S2). The R_g distributions of $A\beta_{42}$ when the protein coexists with the designed peptide P_b showed an extra population with an extended conformation centered at 2.4 nm (Figure 4c). The HDX-MS results and R_g distribution data indicate that P_b induces $A\beta_{42}$ to be extended more than the other two designed peptides (Figures 4a,c). All designed peptides bound to $A\beta_{42}$ without a specific interaction site (Figure 4d). We observed a preference for peptide inhibitors associating with the central hydrophobic region along with the

C-terminal hydrophobic region of $A\beta_{42}$. P_{ab} , which spans both the two hydrophobic regions of $A\beta_{42}$, interacted with Φ_1 and Φ_2 of $A\beta_{42}$ as expected. P_a and P_b , whose sequences correspond to the Φ_1 and Φ_2 regions on $A\beta_{42}$, respectively, also associated with Φ_1 . It is noteworthy that both P_a and P_b interacted with the $A\beta_{42}$ Φ_3 domain. Although P_a and P_b were designed to bind only to their respective Φ_1 and Φ_2 cognate sites on $A\beta_{42}$, we observed that these inhibitors could also concomitantly interact with the Φ_1 and Φ_3 domains of $A\beta_{42}$. Because P_a preferred contact with the Φ_1 domain of $A\beta_{42}$ over the Φ_3 region, P_a showed effective suppression of $A\beta_{42}$ aggregation (Figure S13). On the other hand, P_b still contacts the Φ_1 domain most frequently, but contact probabilities do not differ significantly among the three hydrophobic domains (Figure S13). P_{ab} , which suppressed $A\beta_{42}$ aggregation the most effectively, also made significant contacts with the Φ_2 domain of $A\beta_{42}$, but P_{ab} 's binding to the Φ_1 and Φ_2 domains occurs concomitantly not independently (Figure S14). The

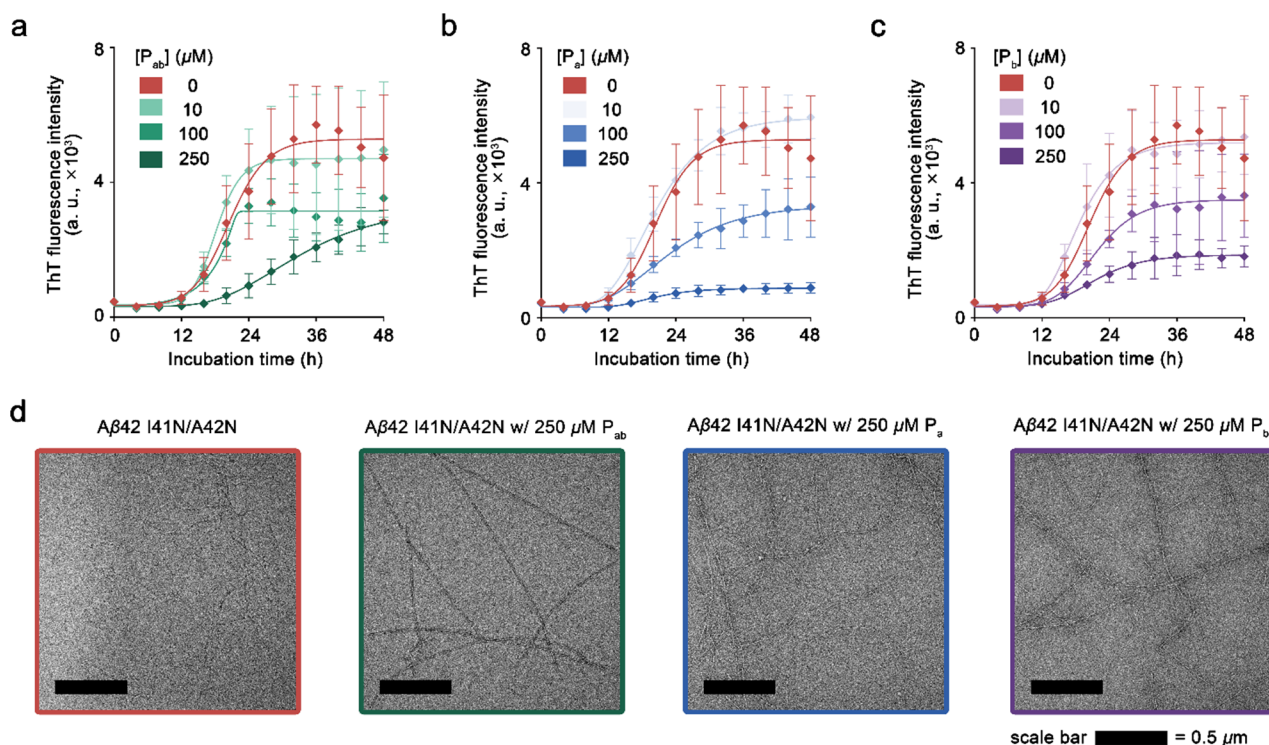


Figure 5. Comparison of amyloid aggregation in mixtures of amyloid- β (1–42) I41N/A42N point mutant and three designed inhibitor candidates. (a–c) ThT fluorescence assay was used to monitor the amyloid aggregation of (a) amyloid- β (1–42) I41N/A42N and mixtures of amyloid- β (1–42) I41N/A42N and P_{ab} , (b) mixtures of amyloid- β (1–42) I41N/A42N and P_a , and (c) mixtures of amyloid- β (1–42) I41N/A42N and P_b . (d) TEM images of mature fibrils of amyloid- β (1–42) I41N/A42N with and without the designed inhibitor candidates. The error bars represent the standard deviation from three independent experiments.

transient binding of designed peptides into the Φ_3 of A β 42 may disrupt intramolecular contact between Φ_2 and Φ_3 (Figure S15).

We experimentally examined the probable binding sites of A β 42 peptide inhibitors by ETD analysis. We used 1,4-dicyanobenzene to generate anions, and the chemical reaction between the A β 42 cation and radical reagent anion led to peptide backbone cleavage. The ETD-MS results revealed that the peptide inhibitors were located around multiple regions of A β 42 (Figure 4e). Structural analysis of A β 42 and inhibitor complexes suggests that P_a and P_b could interact with A β 42 in two different hydrophobic regions (Φ_1 and Φ_3 , respectively). Although we found that P_a and P_b could each separately occupy the Φ_1 and Φ_3 A β 42 sites at the same time, the binding of the designed peptides to different regions may lead to structural conversion of A β 42 to different extents. Taken together, interaction of the designed peptides with the specific hydrophobic region of A β 42 leads to conformational changes and suppresses protein aggregation.

In summary, the designed peptides interacted with A β 42 in multiple hydrophobic domains. The P_{ab} inhibitor associated with the Φ_1 and Φ_2 regions of A β 42, whereas the other peptides interacted with Φ_1 and Φ_3 . Since binding of either P_{ab} or P_a leads to the extension of A β 42 to a similar degree and conveys an inhibitory effect on fibrillar amyloid aggregation, we are prompted to conclude that the Φ_1 domain on A β 42 is likely the main target for suppression of amyloid aggregation (Figures 1c, 2a, and 4). These results also demonstrate that binding of inhibitor candidates to the C-terminus of A β 42 results in an extension of the A β 42 conformation and cannot effectively disrupt fibrillar amyloid aggregation (Figures 2b and

4). The AlphaFold-predicted binding sites of F_a and F_b in prefibrillar A β 42 are also the central hydrophobic regions of the protein. This implies a potential competition for interactions near the central hydrophobic region, where they may also bind adjacent A β 42 molecules in the amyloid fibrils, inducing A β 42 fibril disassembly (Figure 1b).¹⁵

Examination of the Role of Three Key Domains in A β 42 Self-Assembly

Multiple lines of experimental evidence have indicated that Φ_1 is the main target for inhibition of fibrillar amyloid aggregation. Based on the SAXS experiment, we hypothesized that Φ_1 would be shielded by Φ_2 , thereby delaying fibrillar amyloid aggregation, whereas this shielding effect would be weakened when the Φ_2 domain interacted with Φ_3 . To test our hypothesis, we used a double point mutant of A β 42 (I41N/A42N) in order to disrupt the association between the Φ_2 and Φ_3 regions on A β 42. It is commonly accepted that the two hydrophobic residues at the C-terminal end of A β 42 enhance the initiation of the fibrillar amyloid aggregation process compared to A β 40.⁷ The ThT fluorescence assay was performed to compare the fibrillation kinetics between A β 42 and the double point mutant isoform (A β 42 I41N/A42N) in the same peptide concentration (Figure S17). We observed that the point mutations caused a significant kinetical delay in fibrillar amyloid aggregation ($t_{1/2, A\beta 42} = 11.37 \pm 0.82$ h and $t_{1/2, A\beta 42 I41N/A42N} = 22.07 \pm 1.69$ h).

Moreover, we revealed that the hydrophobic interaction-driven binding of the designed peptides (P_a and P_b) was separated into multiple sites, including Φ_1 and Φ_3 (Figure 4d,e). To investigate the effects of focusing the binding of designed peptides into Φ_1 and eliminating competition for this

domain, we applied the designed inhibitors to the A β 42 I41N/A42N mutant. We traced the aggregation kinetics of mixtures of the double point mutant (A β 42 I41N/A42N) and three designed inhibitor candidates. P_{ab} and P_a still had an inhibitory effect on fibrillar amyloid aggregation in a concentration-dependent manner (Figure 5a,b). In addition, P_b, which failed to abolish the fibrillar amyloid aggregation of wild-type A β 42, did suppress the process effectively in the mutant isoform (Figure 5c). The TEM image analysis results were in close agreement with those of the ThT incubation assay (Figure 5d).

Interestingly, all three inhibitor candidates showed inhibitory effects to a similar degree, in contrast to wild-type A β 42 amyloid aggregation (Figures 1 and 2). We confirmed that the conformations of the complex ion (A β 42 I41N/A42N-P_b) merged into a single distribution in the gas phase of the IM spectra (Figure S18). These findings indicate that focusing the binding of designed peptides to Φ_1 suppresses fibrillar amyloid aggregation, highlighting Φ_1 as the primary target for suppressing A β 42 aggregation. Our previous study, which reported the structural difference between A β 40 and A β 42, also suggests that absence of the C-terminal end enhances the interaction between the central hydrophobic and the C-terminal hydrophobic regions, thereby increasing the population of compact conformers of A β 40 compared to A β 42.⁴² Since the central hydrophobic region has been reported to be the key region for initiating A β 40 aggregation as well, the limited role of the C-terminal end of A β 42 on fibrillar amyloid aggregation was observed in comparison with that of both A β 42 I41N/A42N and A β 40.^{43,44}

CONCLUSIONS

In this work, we investigated the roles of the central (¹⁷LVF¹⁹, Φ_1) and C-terminal hydrophobic (³²IGL³⁴, Φ_2) regions, as well as the C-terminal end (⁴¹IA⁴², Φ_3) of A β 42 in the fibrillar amyloid aggregation process, using A β 42 fragments. Taken together, our computational and experimental data suggest that: (1) the Φ_1 domain drives A β 42 amyloid aggregation and that (2) the Φ_2 A β 42 site can interact with either Φ_1 or Φ_3 . If Φ_3 is absent or is replaced by hydrophilic residues, then Φ_2 constantly (yet transiently) interacts with Φ_1 , which disrupts early-stage oligomerization. When Φ_3 is involved in hydrophobic interactions, this preferentially binds to Φ_2 , in turn increasing the likelihood of the Φ_1 domain being more exposed to solvent molecules. This exposure can lead to intermolecular hydrophobic interactions, which drive the oligomerization of A β 42.

Our HDX-MS experiments revealed that nonspecific binding of designed peptides to A β 42 induces the conversion of the A β 42 structure to a more extended conformation, which is related to a lack of intramolecular hydrophobic interactions. Based on structural analyses of A β 42 complexes using IM-MS, REMD simulations, and ETD-MS, we also observed that binding of the designed peptides to the Φ_1 domain of A β 42 suppresses fibrillar A β 42 aggregation. This compelling evidence suggests that the designed peptides' association with the Φ_1 domain of A β 42 can disrupt intermolecular interactions, thereby interfering with A β 42 cluster formation. Furthermore, we identified intramolecular interactions of A β 42 using SAXS and MD simulations. The structural analysis results indicated that intramolecular hydrophobic interactions of the Φ_2 A β 42 site determine the monomeric A β 42 conformation and accessibility to the Φ_1 domain of the protein. To assess the consequent implications on A β 42

aggregation, we monitored the effects of substituting the C-terminal end with a polar amino acid using the A β 42 I41N/A42N mutant and focusing the intramolecular interactions of Φ_2 to the Φ_1 domain. Our findings revealed that the aggregation kinetics of the double point mutant were delayed compared to that of wild-type A β 42.

Because the A β 42 I41N/A42N mutant and A β 40 share similar features during the kinetical delay of fibrillar amyloid aggregation, we suggest that the probable role of the A β 42 C-terminal end is to interfere with the interaction between Φ_1 and Φ_2 . We also observed the binding of the designed inhibitor candidates to A β 42 by combining the MD simulations with MS-based analysis. Multiple lines of evidence indicate that disruption of interpeptide interactions between the Φ_1 domains suppresses the self-assembly properties of A β 42. The Φ_2 A β 42 site is not involved in catalyzing the formation of early-stage oligomers but, conversely, slows down the fibrillar amyloid aggregation process of A β 42. We previously reported that the double point mutation I32N/L34N of A β 42 promotes the self-assembly of the protein.¹⁴

Based on our findings, we designed potential inhibitors of A β 42 amyloid aggregation. Our hypothesis was simple: if the inhibitor reduces the likelihood of the Φ_1 domain being exposed, then oligomerization (and fibrillation) may be hampered. The key hydrophobic residues (F19 and I32) of the A β 42 fragments were replaced by asparagine, which disrupted the alignment of the different A β 42 chains. The designed peptides, P_{ab} and P_a, both of which spanned the Φ_1 domain, could suppress fibrillar amyloid aggregation while alleviating the cytotoxicity of A β 42 and promoting the disassembly of preformed fibrils. In contrast, another designed peptide, P_b, which lacks the Φ_1 domain, failed to disrupt the self-assembly properties of A β 42.

A higher preference for interacting with the Φ_1 domain leads to the effective suppression of fibrillar amyloid aggregation in the context of drug discovery. Our findings herein prompt us to suggest that the seven-residue peptide, P_a, could be a viable candidate as a therapeutic agent that may be further tested in preclinical models. Furthermore, this peptide inhibitor could also be potentially utilized in drug development as an adjuvant to existing therapeutic strategies, such as antibodies and molecular receptors, in order to increase biocompatibility, improve delivery techniques, and enhance the target molecule's binding affinity for the Φ_1 domain of A β 42. Although binding of P_a to the Φ_1 domain of A β 42 suppresses protein aggregation, it may interact with A β 42 in multiple domains competitively. According to our findings, competitive binding reduces the efficacy of P_a; thus, combining it with other approaches that increase selectivity to the Φ_1 domain of A β 42 would be helpful to overcome its limitations.

Our proposed target domain may additionally be used in other types of drug design, including small-molecule inhibitors. Overall, our approaches for investigating inter- and intramolecular interactions and binding with multiple IDP binding sites may be utilized in the development of alternative candidate drugs against several amyloid-deposition neuropathology.

ASSOCIATED CONTENT

Supporting Information

The Supporting Information is available free of charge at <https://pubs.acs.org/doi/10.1021/jacsau.2c00668>.

Additional experimental details, materials, and methods, including photographs of experimental setup (PDF)

AUTHOR INFORMATION

Corresponding Authors

Jeong-Mo Choi – Department of Chemistry, Pusan National University, Busan 46241, Republic of Korea; Chemistry Institute for Functional Materials, Pusan National University, Busan 46241, Republic of Korea; Email: jmchoi@pusan.ac.kr

Hugh I. Kim – Department of Chemistry, Korea University, Seoul 02841, Republic of Korea; Center for Proteogenome Research and Single Cell Analysis Laboratory, Korea University, Seoul 02841, Republic of Korea; orcid.org/0000-0001-9205-1806; Email: hughkim@korea.ac.kr

Authors

Dongjoon Im – Department of Chemistry, Korea University, Seoul 02841, Republic of Korea; Center for Proteogenome Research and Single Cell Analysis Laboratory, Korea University, Seoul 02841, Republic of Korea; orcid.org/0000-0002-6206-657X

Soohyeong Kim – Department of Chemistry, Korea University, Seoul 02841, Republic of Korea; Center for Proteogenome Research and Single Cell Analysis Laboratory, Korea University, Seoul 02841, Republic of Korea

Gyusub Yoon – Department of Chemistry, Korea University, Seoul 02841, Republic of Korea; Center for Proteogenome Research and Single Cell Analysis Laboratory, Korea University, Seoul 02841, Republic of Korea

Da Gyeong Hyun – Department of Chemistry, Korea University, Seoul 02841, Republic of Korea; Center for Proteogenome Research and Single Cell Analysis Laboratory, Korea University, Seoul 02841, Republic of Korea

Yu-Gon Eom – Department of Chemistry, Pusan National University, Busan 46241, Republic of Korea

Ye Eun Lee – Department of Chemistry, Korea University, Seoul 02841, Republic of Korea; orcid.org/0000-0001-7151-1009

Chang Ho Sohn – Center for Nanomedicine, Institute for Basic Science (IBS), Seoul 03722, Republic of Korea; Graduate Program in Nanobiomedical Engineering, Advanced Science Institute, Yonsei University, Seoul 03722, Republic of Korea; orcid.org/0000-0002-7585-1841

Complete contact information is available at:
<https://pubs.acs.org/10.1021/jacsau.2c00668>

Notes

The authors declare no competing financial interest.

ACKNOWLEDGMENTS

This research was supported by a National Research Foundation (NRF) grant, funded by the Korean government (MSIT) (2019R1A2C2086193 and 2021R1A4A1032114 to H.I.K., 2021R1C1C1010943 and 2022R1A4A1033471 to J.-M.C., and 2021R1C1C1004092 and 2021H1D3A2A02096517 to C.H.S.), as well as the Korea Basic Science Institute (KBSI), National Research Facilities & Equipment Center (NFEC), funded by the Korean government (Ministry of Education) (2019R1A6C1010028, and 2020R1A6C103A027 to H.I.K.), and the Korea Health Technology R&D Project through the Korea Health Industry Development Institute (KHIDI) and

Korea Dementia Research Center (KDRC), funded by the Ministry of Health & Welfare, Ministry of Science and ICT, Republic of Korea (grant number: HU21C0071 to H.I.K.) and Institute for Basic Science (IBS-R026-D1 to C.H.S.). Synchrotron X-ray scattering measurements at the 4C SAXS II beamline of the Pohang Accelerator Laboratory were supported by the Ministry of Education and Science Technology of Korea. This work was also supported by the National Institute of Supercomputing and Network/Korea Institute of Science and Technology Information with supercomputing resources, including technical support (KSC-2021-RND-0060 and KSC-2022-CRE-0341). The authors thank the National Center for Seoul National University Research Facilities for their assistance with the TEM measurements.

REFERENCES

- (1) Soto, C. Unfolding the role of protein misfolding in neurodegenerative diseases. *Nat. Rev. Neurosci.* **2003**, *4*, 49–60.
- (2) Glenner, G. G.; Wong, C. W. Alzheimer's disease: Initial report of the purification and characterization of a novel cerebrovascular amyloid protein. *Biochem. Biophys. Res. Commun.* **1984**, *120*, 885–890.
- (3) Goedert, M.; Spillantini, M. G.; Jakes, R.; Rutherford, D.; Crowther, R. A. Multiple isoforms of human microtubule-associated protein tau: sequences and localization in neurofibrillary tangles of Alzheimer's disease. *Neuron* **1989**, *3*, 519–526.
- (4) Roher, A. E.; Lowenson, J. D.; Clarke, S.; Woods, A. S.; Cotter, R. J.; Gowing, E.; Ball, M. J. beta-Amyloid-(1-42) is a major component of cerebrovascular amyloid deposits: implications for the pathology of Alzheimer disease. *Proc. Natl. Acad. Sci. U. S. A.* **1993**, *90*, 10836–10840.
- (5) Sims, R.; Hill, M.; Williams, J. The multiplex model of the genetics of Alzheimer's disease. *Nat. Neurosci.* **2020**, *23*, 311–322.
- (6) Selkoe, D. J.; Wolfe, M. S. Presenilin: Running with Scissors in the Membrane. *Cell* **2007**, *131*, 215–221.
- (7) Jarrett, J. T.; Berger, E. P.; Lansbury, P. T. The carboxy terminus of the .beta. amyloid protein is critical for the seeding of amyloid formation: Implications for the pathogenesis of Alzheimer's disease. *Biochemistry* **1993**, *32*, 4693–4697.
- (8) Cohen, S. I. A.; Linse, S.; Luheshi, L. M.; Hellstrand, E.; White, D. A.; Rajah, L.; Otzen, D. E.; Vendruscolo, M.; Dobson, C. M.; Knowles, T. P. J. Proliferation of amyloid- β 42 aggregates occurs through a secondary nucleation mechanism. *Proc. Natl. Acad. Sci. U. S. A.* **2013**, *110*, 9758–9763.
- (9) Hardy, J. A.; Higgins, G. A. Alzheimer's Disease: The Amyloid Cascade Hypothesis. *Science* **1992**, *256*, 184–185.
- (10) Dubois, B.; Feldman, H. H.; Jacova, C.; Hampel, H.; Molinuevo, J. L.; Blennow, K.; DeKosky, S. T.; Gauthier, S.; Selkoe, D.; Bateman, R.; Cappa, S.; Crutch, S.; Engelborghs, S.; Frisoni, G. B.; Fox, N. C.; Galasko, D.; Habert, M.-O.; Jicha, G. A.; Nordberg, A.; Pasquier, F.; Rabinovici, G.; Robert, P.; Rowe, C.; Salloway, S.; Sarazin, M.; Epelbaum, S.; de Souza, L. C.; Vellas, B.; Visser, P. J.; Schneider, L.; Stern, Y.; Scheltens, P.; Cummings, J. L. Advancing research diagnostic criteria for Alzheimer's disease: the IWG-2 criteria. *Lancet Neurol.* **2014**, *13*, 614–629.
- (11) Aisen, P. S.; Vellas, B.; Hampel, H. Moving towards early clinical trials for amyloid-targeted therapy in Alzheimer's disease. *Nat. Rev. Drug Discovery* **2013**, *12*, 324–324.
- (12) Cummings, J.; Lee, G.; Zhong, K.; Fonseca, J.; Taghva, K. Alzheimer's disease drug development pipeline: 2021. *Alzheimer's Dement.: Transl. Res. Clin. Interv.* **2021**, *7*, No. e12179.
- (13) Michaels, T. C. T.; Šarić, A.; Meisl, G.; Heller, G. T.; Curk, S.; Arosio, P.; Linse, S.; Dobson, C. M.; Vendruscolo, M.; Knowles, T. P. J. Thermodynamic and kinetic design principles for amyloid-aggregation inhibitors. *Proc. Natl. Acad. Sci. U. S. A.* **2020**, *117*, 24251–24257.

- (14) Im, D.; Heo, C. E.; Son, M. K.; Park, C. R.; Kim, H. I.; Choi, J.-M. Kinetic Modulation of Amyloid- β (1–42) Aggregation and Toxicity by Structure-Based Rational Design. *J. Am. Chem. Soc.* **2022**, *144*, 1603–1611.
- (15) Seidler, P. M.; Murray, K. A.; Boyer, D. R.; Ge, P.; Sawaya, M. R.; Hu, C. J.; Cheng, X.; Abskharon, R.; Pan, H.; DeTure, M. A.; Williams, C. K.; Dickson, D. W.; Vinters, H. V.; Eisenberg, D. S. Structure-based discovery of small molecules that disaggregate Alzheimer's disease tissue derived tau fibrils in vitro. *Nat. Commun.* **2022**, *13*, 5451.
- (16) Aprile, F. A.; Sormanni, P.; Perni, M.; Arosio, P.; Linse, S.; Knowles, T. P. J.; Dobson, C. M.; Vendruscolo, M. Selective targeting of primary and secondary nucleation pathways in A β 42 aggregation using a rational antibody scanning method. *Sci. Adv.* **2017**, *3*, No. e1700488.
- (17) Cawood, E. E.; Karamanos, T. K.; Wilson, A. J.; Radford, S. E. Visualizing and trapping transient oligomers in amyloid assembly pathways. *Biophys. Chem.* **2021**, *268*, No. 106505.
- (18) Nguyen, P. H.; Ramamoorthy, A.; Sahoo, B. R.; Zheng, J.; Fallor, P.; Straub, J. E.; Dominguez, L.; Shea, J.-E.; Dokholyan, N. V.; De Simone, A.; Ma, B.; Nussinov, R.; Najafi, S.; Ngo, S. T.; Loquet, A.; Chiricotto, M.; Ganguly, P.; McCarty, J.; Li, M. S.; Hall, C.; Wang, Y.; Miller, Y.; Melchionna, S.; Habenstein, B.; Timr, S.; Chen, J.; Hnath, B.; Strodel, B.; Kaye, R.; Lesné, S.; Wei, G.; Sterpone, F.; Doig, A. J.; Derreumaux, P. Amyloid Oligomers: A Joint Experimental/Computational Perspective on Alzheimer's Disease, Parkinson's Disease, Type II Diabetes, and Amyotrophic Lateral Sclerosis. *Chem. Rev.* **2021**, *121*, 2545–2647.
- (19) Fatafta, H.; Kav, B.; Bundschuh, B. F.; Loschwitz, J.; Strodel, B. Disorder-to-order transition of the amyloid- β peptide upon lipid binding. *Biophys. Chem.* **2022**, *280*, No. 106700.
- (20) Morgan, G. J. Transient disorder along pathways to amyloid. *Biophys. Chem.* **2022**, *281*, No. 106711.
- (21) Jumper, J.; Evans, R.; Pritzel, A.; Green, T.; Figurnov, M.; Ronneberger, O.; Tunyasuvunakool, K.; Bates, R.; Židek, A.; Potapenko, A.; Bridgland, A.; Meyer, C.; Kohl, S. A. A.; Ballard, A. J.; Cowie, A.; Romera-Paredes, B.; Nikolov, S.; Jain, R.; Adler, J.; Back, T.; Petersen, S.; Reiman, D.; Clancy, E.; Zielinski, M.; Steinegger, M.; Pacholska, M.; Berghammer, T.; Bodenstein, S.; Silver, D.; Vinyals, O.; Senior, A. W.; Kavukcuoglu, K.; Kohli, P.; Hassabis, D. Highly accurate protein structure prediction with AlphaFold. *Nature* **2021**, *596*, 583–589.
- (22) Pettersen, E. F.; Goddard, T. D.; Huang, C. C.; Couch, G. S.; Greenblatt, D. M.; Meng, E. C.; Ferrin, T. E. UCSF Chimera—A visualization system for exploratory research and analysis. *J. Comput. Chem.* **2004**, *25*, 1605–1612.
- (23) Kwang-Woo, K.; Jehan, K.; Young Duck, Y.; Hyungju, A.; Byoungseok, M.; Na Hyung, K.; Seungyu, R.; Hyo-Yun, K.; Chae-Soon, L.; In Deuk, S.; Woul-Woo, L.; Hyeong Joo, C.; Kyeong Sik, J. Small-angle X-ray Scattering Beamline BL4C SAXS at Pohang Light Source II. *BioDesign* **2017**, *5*, 24–29.
- (24) Manalastas-Cantos, K.; Konarev, P. V.; Hajizadeh, N. R.; Kikhney, A. G.; Petoukhov, M. V.; Molodenskiy, D. S.; Panjkovich, A.; Mertens, H. D. T.; Gruzinov, A.; Borges, C.; Jeffries, C. M.; Svergun, D. I.; Franke, D. ATSAS 3.0: expanded functionality and new tools for small-angle scattering data analysis. *J. Appl. Crystallogr.* **2021**, *54*, 343–355.
- (25) Van Der Spoel, D.; Lindahl, E.; Hess, B.; Groenhof, G.; Mark, A. E.; Berendsen, H. J. C. GROMACS: Fast, flexible, and free. *J. Comput. Chem.* **2005**, *26*, 1701–1718.
- (26) Huang, J.; Rauscher, S.; Nawrocki, G.; Ran, T.; Feig, M.; de Groot, B. L.; Grubmüller, H.; MacKerell, A. D. CHARMM36m: an improved force field for folded and intrinsically disordered proteins. *Nat. Methods* **2017**, *14*, 71–73.
- (27) Jorgensen, W. L.; Chandrasekhar, J.; Madura, J. D.; Impey, R. W.; Klein, M. L. Comparison of simple potential functions for simulating liquid water. *J. Chem. Phys.* **1983**, *79*, 926–935.
- (28) Onufriev, A.; Bashford, D.; Case, D. A. Exploring protein native states and large-scale conformational changes with a modified generalized born model. *Proteins: Struct., Funct., Bioinf.* **2004**, *55*, 383–394.
- (29) Gremer, L.; Schölzel, D.; Schenk, C.; Reinartz, E.; Labahn, J.; Ravelli, R. B. G.; Tusche, M.; Lopez-Iglesias, C.; Hoyer, W.; Heise, H.; Willbold, D.; Schröder, G. F. Fibril structure of amyloid- β (1–42) by cryo-electron microscopy. *Science* **2017**, *358*, 116–119.
- (30) Tao, K.; Wang, J.; Zhou, P.; Wang, C.; Xu, H.; Zhao, X.; Lu, J. R. Self-Assembly of Short A β (16–22) Peptides: Effect of Terminal Capping and the Role of Electrostatic Interaction. *Langmuir* **2011**, *27*, 2723–2730.
- (31) Yankner, B. A.; Duffy, L. K.; Kirschner, D. A. Neurotrophic and Neurotoxic Effects of Amyloid β Protein: Reversal by Tachykinin Neuropeptides. *Science* **1990**, *250*, 279–282.
- (32) Borghesani, V.; Alies, B.; Hureau, C. Cu(II) binding to various forms of amyloid- β peptides. Are they friends or foes? *Eur. J. Inorg. Chem.* **2018**, *2018*, 7–15.
- (33) Flood, J. F.; Morley, J. E.; Roberts, E. An amyloid β -protein fragment, A β [12–28], equipotently impairs post-training memory processing when injected into different limbic system structures. *Brain Res.* **1994**, *663*, 271–276.
- (34) Baumketner, A.; Bernstein, S. L.; Wyttenbach, T.; Lazo, N. D.; Teplow, D. B.; Bowers, M. T.; Shea, J. E. Structure of the 21–30 fragment of amyloid beta-protein. *Protein Sci.* **2006**, *15*, 1239–1247.
- (35) Reddy, A. S.; Izmitli, A.; de Pablo, J. J. Effect of trehalose on amyloid β (29–40)-membrane interaction. *J. Chem. Phys.* **2009**, *131*, No. 085101.
- (36) Cheng, L.; Yin, W. J.; Zhang, J. F.; Qi, J. S. Amyloid beta-protein fragments 25–35 and 31–35 potentiate long-term depression in hippocampal CA1 region of rats in vivo. *Synapse* **2009**, *63*, 206–214.
- (37) Hernandez-Guillamon, M.; Mawhirt, S.; Blais, S.; Montaner, J.; Neubert, T. A.; Rostagno, A.; Ghiso, J. Sequential Amyloid- β Degradation by the Matrix Metalloproteases MMP-2 and MMP-9. *J. Biol. Chem.* **2015**, *290*, 15078–15091.
- (38) Yan, P.; Hu, X.; Song, H.; Yin, K.; Bateman, R. J.; Cirrito, J. R.; Xiao, Q.; Hsu, F. F.; Turk, J. W.; Xu, J.; Hsu, C. Y.; Holtzman, D. M.; Lee, J.-M. Matrix Metalloproteinase-9 Degrades Amyloid- β Fibrils in Vitro and Compact Plaques in Situ. *J. Biol. Chem.* **2006**, *281*, 24566–24574.
- (39) Mazzitelli, S.; Filipello, F.; Rasile, M.; Lauranzano, E.; Starvaggi-Cucuzza, C.; Tamborini, M.; Pozzi, D.; Barajon, I.; Giorgino, T.; Natalello, A.; Matteoli, M. Amyloid- β 1–24 C-terminal truncated fragment promotes amyloid- β 1–42 aggregate formation in the healthy brain. *Acta Neuropathol. Commun.* **2016**, *4*, 110.
- (40) Yong, W.; Lomakin, A.; Kirkitadze, M. D.; Teplow, D. B.; Chen, S.-H.; Benedek, G. B. Structure determination of micelle-like intermediates in amyloid β -protein fibril assembly by using small angle neutron scattering. *Proc. Natl. Acad. Sci. U. S. A.* **2002**, *99*, 150–154.
- (41) Morel, B.; Carrasco, M. P.; Jurado, S.; Marco, C.; Conejero-Lara, F. Dynamic micellar oligomers of amyloid beta peptides play a crucial role in their aggregation mechanisms. *Phys. Chem. Chem. Phys.* **2018**, *20*, 20597–20614.
- (42) Heo, C. E.; Choi, T. S.; Kim, H. I. Competitive homo- and hetero- self-assembly of amyloid- β 1–42 and 1–40 in the early stage of fibrillation. *Int. J. Mass Spectrom.* **2018**, *428*, 15–21.
- (43) Gazit, E. A possible role for π -stacking in the self-assembly of amyloid fibrils. *FASEB J.* **2002**, *16*, 77–83.
- (44) Brender, J. R.; Ghosh, A.; Kotler, S. A.; Krishnamoorthy, J.; Bera, S.; Morris, V.; Sil, T. B.; Garai, K.; Reif, B.; Bhunia, A.; Ramamoorthy, A. Probing transient non-native states in amyloid beta fiber elongation by NMR. *Chem. Commun.* **2019**, *55*, 4483–4486.